Ab initio piezoelectric properties of wurtzite ZnO-based alloys: Impact of the c/a cell ratio

A. Py-Renaudie,[1] P. Daoust,[1] M. Côté,[2] P. Desjardins,[1] and R. A. Masut[1]

[1]*Department of Engineering Physics and Regroupement Québécois sur les Matériaux de Pointe, Polytechnique Montréal, C.P. 6079, Succ. Centre-Ville, Montréal, Québec H3C 3A7, Canada*

[2]*Department of Physics and Regroupement Québécois sur les Matériaux de Pointe, Université de Montréal, C.P. 6128, Succ. Centre-Ville, Montréal, Québec H3C 3J7, Canada*

(Received 3 October 2019; accepted 15 November 2019; published 1 May 2020)

The piezoelectric (PE) and stiffness tensors of 32-atom supercells of ZnO-based alloys have been obtained from *ab initio* simulations using density functional perturbation theory in the local density approximation. Low concentration for substituents to Zn, O, or both were considered in unstrained and biaxially strained supercells. The d_{33} coefficient for unstrained $Zn_{15}YO_{15}N$ and $Zn_{15}LaO_{15}N$ alloys are, respectively, 17.5 and 18 pC N^{-1}, whereas e_{33} is 1.7 C m^{-2} for both alloys. These values are significantly improved compared to simulated values for pristine ZnO ($d_{33} = 11.4$ pC N^{-1} and $e_{33} = 1.3$ C m^{-2}). Applying 2% tensile strain on $Zn_{15}YO_{15}N$ results in an increase of the e_{33} coefficient to 2.1 C m^{-2}, a 62% increase over the value calculated for pristine ZnO. We confirm for a variety of ternary and quaternary ZnO-based alloys that a linear relation is verified between the e_{33} coefficient and the cell ratio c/a, described by a slope ≈ -9 C m^{-2}. Our results also indicate that the PE coefficients follow the same trends with respect to changes in c/a caused by variations in chemical composition or by applying biaxial strain. Based on this correlation, we propose a simple method to identify promising candidates among piezoelectric alloys in the wurtzite family, effectively reducing the intensive computational resources needed to obtain optimal PE performance for applications compatible with the many requirements of thin film growth and processing.

DOI: 10.1103/PhysRevMaterials.4.053601

I. INTRODUCTION

Piezoelectricity is a phenomenon entailing the direct conversion of mechanical deformation into changes of the electrical polarization and vice versa. It allows for the fabrication of various devices such as transducers [1], resonators [2], surface acoustic wave devices (SAW) [3,4], and piezoelectric (PE) energy harvesters [5]. The most common PE materials for thin film applications are lead-based (Pb), such as PZT (lead zirconate titanate) [4,6]. Because of the high toxicity of Pb, significant efforts have been devoted to develop lead-free PE materials [7].

ZnO, a wide band gap semiconductor, is a promising nontoxic alternative PE material. It possesses one of the strongest PE strain coefficient d_{33} among tetrahedrally bonded binary semi-conductors (12 pC N^{-1}) while magnetron sputtering allows for the deposition of high crystalline quality films. The PE performances of ZnO remain, however, one or two orders of magnitude below that of state of the art PZT ferroelectrics. It is therefore critical to find ways to improve the PE properties of ZnO to extend its range of applications. Recent experimental [8–12] and theoretical [13,14] studies of ZnO-based alloys suggest that the PE coefficients increase with alloying concentration and tensile strain as long as the materials remains in the wurtzite phase. These studies also indicate that the nature of the alloying elements also impacts the PE coefficients. So far, investigation of PE properties of ZnO alloys relied on DFPT calculations carried out without a clear consensus nor theoretical predictions to choose the potential candidates.

Consequently, we have carried out a systematic investigation of the PE properties of more than a dozen low-concentration ternary and quaternary ZnO-based alloys using the density functional perturbation theory (DFPT) method [15]. DFPT calculations are able to provide the entire PE and elastic tensors and therefore allow for a more complete analysis of these interrelated properties. We focused primarily on the transverse PE coefficients (d_{33} and e_{33} in the Voigt notation), often used as the main PE coefficients of interest in the case of resonators; and structural parameters (in particular the lattice cell ratio c/a). Our results reveal a negative-slope linear relationship between e_{33} and the cell ratio c/a for these low concentration alloys, as was previously shown for pristine wurtzite materials [13], independent of the nature of the alloying element. That linear relationship allows for a rapid qualitative prediction of the PE performances of a large variety of alloys, with the best performances obtained for smaller c/a values as was already proposed by Momida and Oguchi [13].

We also show, using $Zn_{15}YO_{15}N$ alloys as a model system, that the PE coefficients follow the same linear trends with respect to changes in c/a caused by applying biaxial strain. It was also observed that, for the range of c/a values investigated for this biaxially strained model system, the stiffness coefficient C_{33} increases almost linearly with increasing c/a values. Further analysis for higher alloying concentrations suggest that the PE coefficient becomes largest when approaching the structural phase transition from wurtzite ton nonpolar hexagonal structure. The observed linear relationship between e_{33} and c/a allows for a rapid systematic screening of ZnO-based

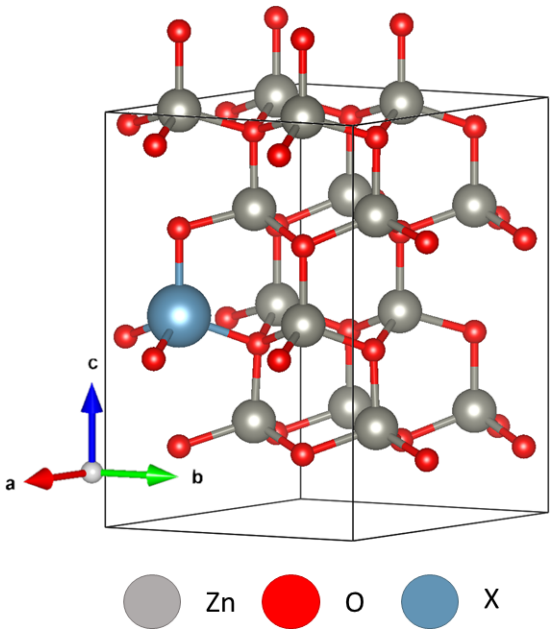

FIG. 1. Schematic representation of a typical simulated $Zn_{15}XO_{16}$ alloy supercell (X refers to the Zn substituent, depending on the alloy) rendered with the VESTA software based on structural parameters calculated following a DFT relaxation process.

alloys of potential interest, through less intensive structural analysis. Indeed, we calculated and analyzed c/a values for almost 40 ternary and quaternary alloys using straightforward DFT calculations and identified the most promising candidates based on their predicted e_{33} coefficients.

II. METHODOLOGY

The DFT and DFPT calculations were carried out using the ABINIT software [16], in conjunction with the local density approximation (LDA) since, at present, DFPT calculations in ABINIT are restricted to this framework under the PAW formalism. We used in this work the version 8.4.4 of ABINIT. DFPT calculations using the GGA functional are implemented in ABINIT for norm conserving pseudopotentials. The LDA functional is simpler and easier to implement when compared to GGA, an extension to LDA. We used the JTH library [17] under the PAW formalism [18,19] as atomic datasets. Wurtzite $2 \times 2 \times 2$ supercells (32 atoms), some of which were under -1% to $+2\%$ in plane strain constituted the simulation domain as represented schematically in Fig. 1. An energy cutoff of 25 Hartree ($\sim$680 eV) and a $4 \times 4 \times 4$ Monkhorst-Pack grid [20] were chosen based on a convergence study to limit numerical errors under 1% for e_{33} and d_{33} values. The starting alloy configuration is allowed to relax following a Broyden-Fletcher-Goldfarb-Shanno (BFGS) minimization algorithm [21]. For the investigation of the influence of strain, the supercell is biaxally strained in the plane (a and b axes), before being allowed to relax along the c axis without imposing any constraint on the cell volume. We then calculated the band structure, cell parameters, and ground state energy. The PE and stiffness coefficients were calculated in the DFPT formalism, implemented in ABINIT as described in Ref. [15], relying on the modern theory of electrical polarization [22] known as the Berry phase approach.[1]

TABLE I. Comparison between calculated and experimental values of lattice constants and band gap energy for wurtzite ZnO.

	Present study	LDA [25]	GGA [13]	Experiment [36]
a (Å)	3.1838	3.1836	3.29	3.2427
c (Å)	5.1493	5.1497	5.30	5.1948
$\boldsymbol{c/a}$	1.617	1.617	1.611	1.602
Volume (Å^3)	45.203	45.202	49.68	47.306
Band gap (eV)	0.793	0.796	0.82	3.44

III. RESULTS

We have carried out a systematic investigation of the effects of composition and strain on the computed PE properties of ZnO-based alloy. We begin by presenting the properties of pristine ZnO to establish a solid baseline for the analysis of the results for the alloys.

A. Properties of pristine ZnO

We have first determined the properties of pristine wurtzite ZnO to establish a baseline and validate our calculations. The lattice parameters and the band gap energy obtained from the DFT calculations are presented in Table I, whereas the PE coefficients deduced from DFPT simulations are summarized in Table II.

Our numerical results for both the lattice parameters and the band gap energy (Table I) closely match the simulated values reported by Goh *et al.* [25], as expected since both sets of calculations were carried out with the ABINIT software using the JTH library of datasets under the PAW formalism. The calculated lattice parameters are within 2% of the experimental values; the c/a ratio and the cell volume are underestimated by less than 1% and 4.5%, respectively. As previously pointed out by Goh *et al.* [25], and consistent with previous observations on a number of materials systems (see, e.g., Ref. [26]), DFT calculations using LDA or GGA greatly underestimate band gap energies.

We want to stress that even though the calculated band gap is significantly underestimated, its precise value does not

[1]We have limited our investigation to materials systems that preserve valence neutrality of the supercells since no theoretical work has been developed for implementing DFPT calculations for nonvalence-neutral systems. As described by Bruneval *et al.* [23], this approach has been implemented for DFT (not DFPT) calculations in ABINIT under the PAW formalism. We found, however, that DFPT calculations performed with ABINIT adding neutralizing uniform background charges gave nonreliable results [24]. We note that despite the absence of a solid theoretical framework, Nakamura *et al.* [14] used the VASP software for computing the PE properties of systems requiring the addition of background charges to reach valence neutrality. Taking into consideration non valence-neutral systems allows for a broader range of alloys, an approach that should be investigated in a later study.

TABLE II. Comparison of calculated and experimental values of nonzero piezoelectric stress e_{ij}, piezoelectric strain d_{ij}, and stiffness C_{ij} coefficients in the Voigt notation for wurtzite ZnO.

	Present study	Difference with experiment	LDA [28]	Difference with experiment	GGA + U [14]	Difference with experiment	Experiment [37]
e_{31} (**C m**$^{-2}$)	−0.697	12%	−0.67	8%	−0.51	18%	−0.62
e_{33} (**C m**$^{-2}$)	1.293	35%	1.28	33%	1.04	8%	0.96
e_{15} (**C m**$^{-2}$)	−0.550	49%	−0.53	43%	−0.38	3%	−0.37
C_{11} (GPa)	220	5%	226	8%	203	3%	209
C_{12} (GPa)	139	16%	139	16%	110	8%	120
C_{13} (GPa)	124	19%	123	18%	92	11%	104
C_{33} (GPa)	243	15%	242	15%	210	0.5%	211
C_{44} (GPa)	38	14%	40	9%	43	2%	44
d_{31} (**pC N**$^{-1}$)	−5.81	14%	−5.5	8%	−4.2	18%	−5.1
d_{33} (**pC N**$^{-1}$)	11.4	8%	10.9	11%	8.7	29%	12.3
d_{15} (**pC N**$^{-1}$)	−14.7	75%	−13.1	56%	−8.8	6%	−8.3

impact the computation of the PE and stiffness tensors as long as the simulated material exhibits a finite band gap throughout the entire calculation. Indeed, the polarization (and subsequently the piezoelectricity) is defined only for insulators and semiconductors [27]. However, the DFPT calculation of the PE and stiffness coefficient relies on a perturbative method that does not use the band gap value [28]. It is therefore critical to assess that the calculated band structure exhibits a finite band gap before proceeding with DFPT calculations.

Table II summarizes the most important components of the PE strain (d_{ij}) and stress (e_{ij}) coefficients as well as the stiffness coefficients (C_{ij}). The PE and stiffness results agree very well with previous LDA-based calculations [28]. We attribute the small discrepancies, less than 6% (except for d_{15}), to the fact that these authors used norm conserving pseudopotentials for the simulations (Trouillier-Martins pseudopotentials) [29], whereas PAW potentials are used in the present study.

A direct comparison with the results of Nakamura *et al.* [14], sixth column of Table II, allows for a comparison with GGA + U results. As reported by Nakamura *et al.* [14]. the LDA method slightly underperforms compared to the GGA + U method when compared to the experimental data with the exception of the d_{33} and e_{31} coefficients where the LDA values are closer to the experimental data. Those slight differences are not sufficient, however, to identify a clearly superior approach. Furthermore, the +U method introduces more variability to the study since it requires to calculate the value of the +U parameter for each atom depending on its environment to correct the limitations of the functional [30]. This parameter effectively changes the atomic potential, thus modifying the electronic properties of the system [25] such as the value of the cell ratio c/a, thereby raising concerns when comparing simulations performed for different alloys using different +U parameters.

B. Properties of ZnO-based alloys

Our investigation covers a wide range of ZnO-based alloys to shed light on the physical origin of and mechanism for the improved PE characteristics in these materials. In all cases, we first calculate the structural properties and the band structure, to verify the nonmetallic character of the alloy, which is necessary for carrying out the DFPT simulations of the PE properties as described above. For the systems exhibiting a large enough band gap energy (>0.2 eV), we run DFPT calculations to obtain the PE and stiffness properties (see the Supplemental Material for an example of raw data [31]). Since LDA greatly underestimates band gap energies, it is possible that some potentially promising systems for which the simulation provides a very small gap cannot be directly investigated. As will be discussed below, we confirm for a variety of ternary and quaternary ZnO-based alloys that a linear relation is verified between e_{33} and c/a. We can therefore identify which materials systems, among those having band gap energies too small to allow DFPT calculations, could be of interest.

As indicated in Sec. II, we focused on materials corresponding to valence neutral supercells, starting with $Zn_{15}CdO_{16}$ and $Zn_{15}HgO_{16}$ which are obvious choices for Zn substitution. Similarly, $Zn_{16}O_{15}S$ and $Zn_{16}O_{15}Se$ were considered for O substitution. We also investigated ternary alloys comprising elements of column IIA (the main part of our data) as well as quaternary alloys in which a Zn atom is replaced by a column IIIB metal (Sc, Y, and La) whereas one O atom is replaced by a nitrogen atom to assure that the system is still semiconducting, i.e., the Fermi energy is in the band gap.

In this latter case (quaternary alloys), we chose to study only one substitutional site for the anion: the nearest neighbor of the substituted cation along the z axis (site 1 in Fig. 1). It is to be noted, however, that all anions in the supercell are not equivalents. If one were to study in depth the quaternary alloys, a careful determination of the influence of those sites on the PE properties of the alloys would be necessary, and this falls outside the scope of this study.

The results for all alloys exhibiting a finite band gap energy are summarized in Fig. 2. As indicated in Fig. 2(a), c/a values range from 1.63 for $Zn_{15}BaO_{16}$ to 1.58 for $Zn_{15}YO_{15}N$. The band gap energy values are presented in Fig. 2(b). An important reduction of the band gap energy can be observed for alloy incorporating Cd, Hg, Y(N), La(N), S, and Se. Alloys incorporating Be, Mg, Ca, Sr, and Ba all exhibit a

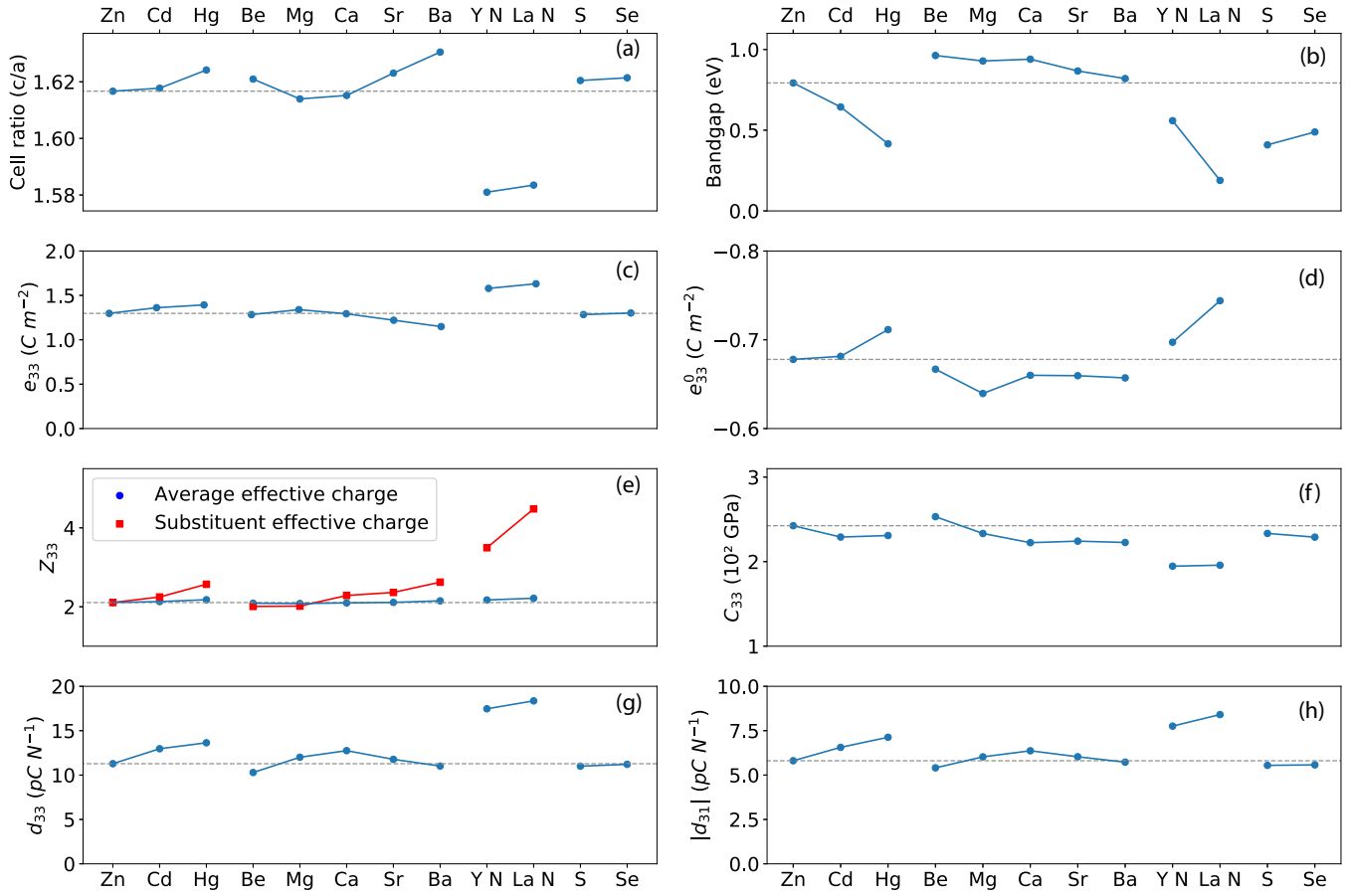

FIG. 2. (a) c/a cell ratio, (b) band gap energy E_g, (c) total piezoelectric stress coefficient e_{33}, (d) clamped piezoelectric stress coefficient e^0_{33}, (e) Born effective charge (dots for the cell average and squares for the substituent), (f) stiffness coefficient C_{33}, (g) total piezoelectric strain coefficient d_{33}, and (h) absolute value of the total piezoelectric stress coefficient d_{31}. All calculations were carried out on $2 \times 2 \times 2$ supercells for ternary $Zn_{15}XO_{16}$ (X = substitute element) and quaternary $Zn_{15}XO_{15}N$ alloys. (A 16-atom alloy, Zn_7YO_7N was simulated with a $1 \times 2 \times 2$ supercell but is not presented here, only in Fig. 3). Data for S and Se are not displayed in (d) and (e) because they are oxygen substituents. Results are grouped by columns of the periodic table.

band gap energy above the calculated band gap energy of pristine ZnO.

The PE properties are described in Fig. 2, which shows (c) the total PE stress coefficient e_{33}, (d) the clamped PE stress coefficient e^0_{33}, (e) the Born effective charge (dots for the cell average and squares for the substituent), (f) the stiffness coefficient C_{33}, (g) the total PE strain coefficient d_{33}, and (h) the absolute value of the total PE stress coefficient d_{31}.

The PE performance vary significantly for the different alloys whether we consider the e_{33} coefficient [Fig. 2(e)] or the d_{33} coefficient [Fig. 2(d)]. The e_{33} coefficient improves for fewer alloys, however, for instance, Cd, Hg, Mg, Y(N), and La(N). The quaternary alloys incorporating Y(N) and La(N) offer the best PE performance.

The stiffness coefficient C_{33} [Fig. 2(f)] is significantly reduced in all alloys except $Zn_{15}BeO_{16}$. The largest decrease is observed for the quaternary systems in which we substituted O with N to maintain charge balance in the supercell for carrying out the DFPT calculations. A further look into the C_{33} coefficient for the $Zn_{15}YO_{15}N$ alloy indicates that it is linearly related to the decrease in c/a in strained systems (see Fig. 2 in the Supplemental Material [31]). Most significantly, the improvement of the d_{33} coefficient in these alloys does not solely arise from a decrease in the stiffness C_{33} coefficient but also from a clear improvement of the e_{33} coefficient [Figs. 2(f) and 2(c)].

A careful examination of Figs. 2(a) and 2(c) reveals that variations in e_{33} and c/a values are correlated, as reported earlier by Momida and Oguchi [13] for a variety of binary and ternary materials with a wurtzite structure. The values of e_{33} are plotted against c/a in Fig. 3. The data is well described by a linear relationship with a slope ≈ -9 C m^{-2}, with a very high coefficient of determination ($R^2 = 0.98$ for unstrained 32-atom systems; strain effects are discussed in Sec. III C).

This result is qualitatively consistent with the work of Momida and Oguchi [13], who obtained a slope of ≈ -19 C m^{-2} when considering a variety of wurtzite materials. An analysis of a subset of their data for $Ca_xZn_{1-x}O$ alloys ($x = 0$–0.25) yields a slope of ≈ -4 to -6 C m^{-2}. At this point we cannot establish the origin of the different slope values. It may be simply related to the wider family of wurtzite materials considered in Ref. [13]. The discrepancy in slopes for the $Ca_xZn_{1-x}O$ alloys may be related to the high concentration of substituent, taking the system further away from pristine ZnO.

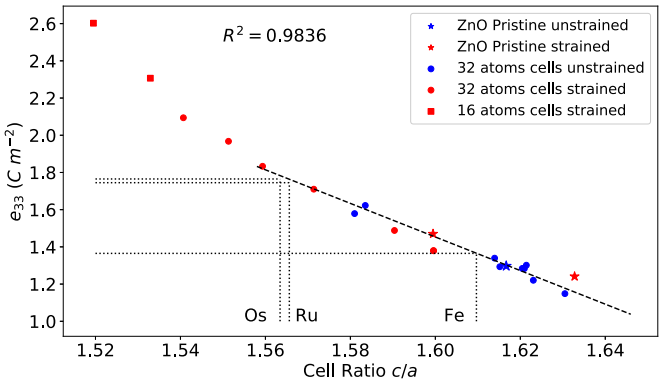

FIG. 3. Calculated e_{33} coefficient vs. c/a cell ratio for ternary $Zn_{15}XO_{16}$ (X = substitute element) and quaternary $Zn_{15}YO_{15}N$ alloys. The straight dashed line, a least-square fit to the unstrained data, has a slope of -9 C m^{-2} with a coefficient of determination of 0.98. The 32-atom strained supercells are for $Zn_{15}YO_{15}N$ alloys and 16 atom- strained supercells refer to Zn_7YO_7N alloys. As explained in the text, it is not possible to calculate the piezoelectric coefficient using DFPT for alloys that do not exhibit a nonzero DFT band gap. The c/a values for three examples of such alloys are indicated using dotted lines, namely, $Zn_{15}FeO_{16}$, $Zn_{15}RuO_{16}$, and $Zn_{15}OsO_{16}$.

C. Strained systems

We carried out an investigation of the effect of in-plane biaxial strain on the PE properties of ZnO and $Zn_{15}YO_{15}N$, to determine, in particular, if variations in c/a caused by strain follow the same trends as those introduced by changing the alloying elements as described in Fig. 3. The range of strain values investigated is within what can be achieved through heteroepitaxial growth [32].

We have first applied a biaxial in-plane strain on a 32 atoms ZnO supercell, allowing the systems to relax freely along the c axis. The results in Fig. 3 show that a tensile (positive) strain (elongation along the a and b axes) leads to a reduction of the ZnO cell ratio c/a, and also to an increase in e_{33}. A negative (compressive) strain leads to an increase in the cell ratio c/a and to a decrease of the e_{33} coefficient. It is crucial to note that the linear trend identified in the previous section is still valid for pristine ZnO under strain. The value obtained for a positive strain follows the same slope as the one obtained with the substituents, as can be seen in Fig. 3. The negative strain value deviates slightly from the prediction of the linear regression, but the difference is small enough to consider that the linear regression obtained with the substituents remains valid in the case of applied strain. The improvement of the PE performance is significant, even for a reasonable 1% strain.

The impact of in-plane strain on the PE properties of $Zn_{15}YO_{15}N$ is presented in Figs. 3 and 4. The application of a 2% biaxial tensile strain results in an e_{33} coefficient of 2.09 C m^{-2}, an increase of 0.5 C m^{-2} compared to the unstrained system. The d_{33} coefficient is further improved and reaches 30 pC N^{-1}, an enhancement of 12.6 pC N^{-1}. In contrast, a 1% biaxial compressive strain enhances the c/a ratio

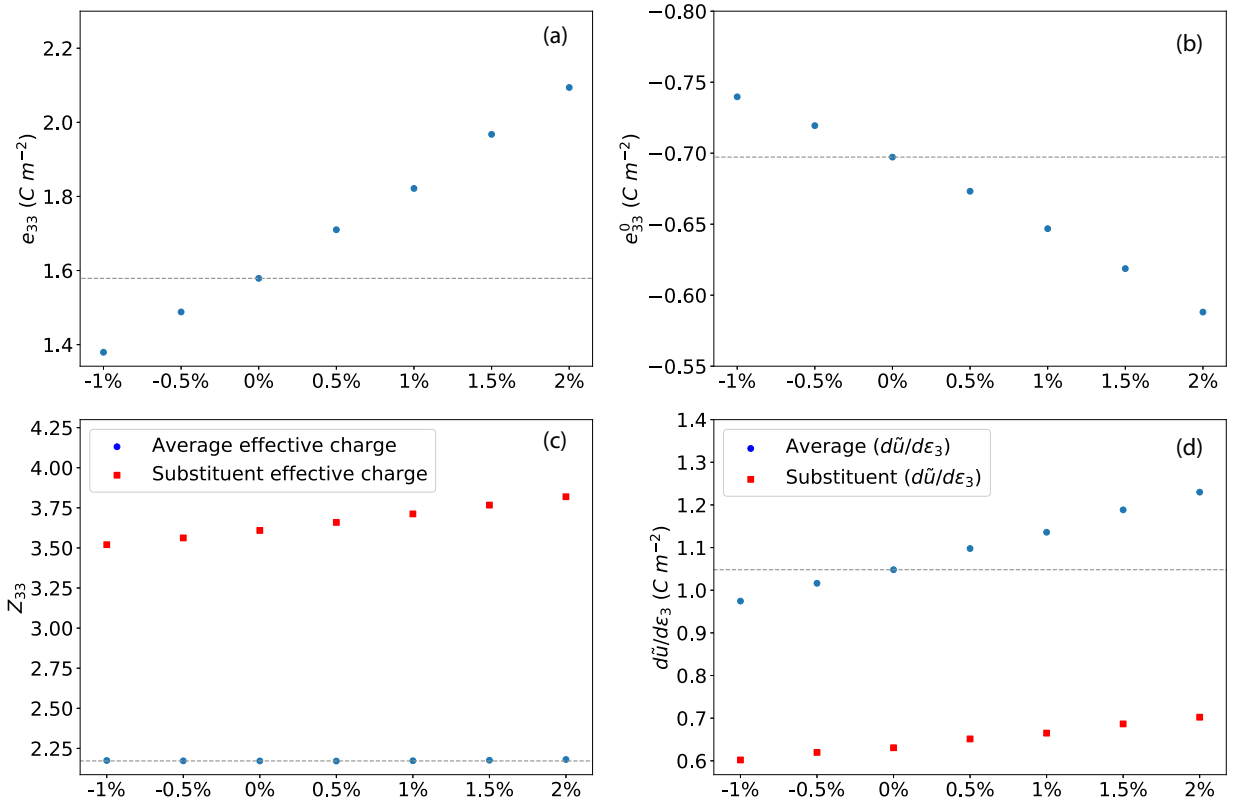

FIG. 4. Evolution of the (a) e_{33} coefficient, and of its components (b) e^0_{33}, (c) Z_{33}, and (d) $\partial\tilde{u}/\partial\varepsilon_3$ as a function of applied strain for $Zn_{15}YO_{15}N$ alloys. The circular symbols represent average values over the supercell, while squares refer to local values associated with the substituent.

and is associated with a decrease in PE performance. At 1% biaxial compressive strain, the e_{33} coefficient for $Zn_{15}YO_{15}N$ is reduced to 1.38 C m^{-2}. The linear relationship between e_{33} and c/a is maintained for these materials systems as was observed previously for pristine ZnO, even though a small variation can be observed at the extrema of our simulation domain as discussed in Sec. IV.

The overall set of results presented in the above subsections strongly suggests a fundamental relationship between e_{33} and c/a. To better understand this relationship, we first decompose the e_{33} coefficient as defined under the linear piezoelectricity formalism [33]. All these quantities are global quantities, defined on average in the supercell. Equations (1) and (2),

$$e_{33} = e_{33}^0 + \frac{\partial P_3}{\partial u}\frac{\partial u}{\partial \epsilon_3}, \tag{1}$$

$$e_{33} = e_{33}^0 + \frac{4e}{\sqrt{3}a^2} Z_{33}\frac{\partial u}{\partial \epsilon_3}, \tag{2}$$

introduce the clamped ion coefficient e_{33}^0 (in C m^{-2}), the Born effective charge Z_{33} (dimensionless), and the variation of the wurtzite parameter, u (dimensionless), with respect to strain $\partial u/\partial \epsilon_3$. In these equations, e is the electron charge and a is the cell parameter. This latter internal relaxation term is a measure of the relative variation of position of the sublattices (u is defined as a dimensionless parameter, measuring the length of the bond between a zinc and an oxygen atom in the c direction) [33].

Introducing the notation $(\partial \tilde{u}/\partial \epsilon_3)$, we can rewrite Eq. (2) as

$$e_{33} = e_{33}^0 + Z_{33}\left(\frac{\partial \tilde{u}}{\partial \epsilon_3}\right) \quad \text{with} \quad \tilde{u} = \frac{4e}{\sqrt{3}a^2}\, u. \tag{3}$$

In the following analysis, we should keep in mind that this last term is not formally defined for supercells.

This decomposition permits to analyze the origin of the variation of the PE coefficient e_{33} by studying its different components. We summarize the results for strained $Zn_{15}YO_{15}N$ alloys in Fig. 4 with (a) the total PE stress coefficient e_{33} (in C m^{-2}), (b) the clamped ion coefficient e_{33}^0 (in C m^{-2}), (c) the Born effective charge Z_{33} (dimensionless), and (d) $(\partial \tilde{u}/\partial \epsilon_3)$ (in C m^{-2}).

As pointed out by Momida and Oguchi [13], it is clear in Fig. 4(b) that the variations due to strain of the clamped ion coefficient e_{33}^0 are not important enough (about 20% of the e_{33} variations) to explain alone the observed improvement in e_{33}. More interestingly, we observe that the average Born effective charge does not vary with strain, even though the local Born effective charge does. We propose that this can be interpreted as a reorganization of the charge distribution in the supercell due to the substitution of a Zn atom or to strain. Thus, the main factor of improvement for PE performance resides in the second term of Eq. (3), which can be understood as the relative movement of the two sublattices under the effect of strain as explained by Dal Corso *et al.* [33].

D. Effect of concentration

To further assess the universality of the linear relationship between e_{33} and c/a observed for substitution and strain, we investigated the impact of concentration of substituents in $Zn_{1-x}Y_xO_{1-x}N_x$ alloys.

In a first set of simulations, the substituent (Y and N) concentration was doubled by reducing the number of atoms in the supercell down to half (16 atoms instead of 32). We chose to reduce the number of atoms in the supercell to avoid taking into considerations the different configurations accessible for a 32 atoms supercell with four substituents (2 Y and 2 N). This approach may not be as accurate, but it renders the calculations more tractable. The relaxation stage for this $Zn_7Y_1O_7N_1$ alloy led to a nonpolar hexagonal structure (with inversion symmetry), which yields no PE properties.

In an attempt to maintain the wurtzite structure at higher concentrations for these material systems, we applied a compressive biaxial strain of -0.5 and -1.0% to $Zn_7Y_1O_7N_1$ alloys. In both cases, the system with applied strain converged to a wurtzite structure. The results of the e_{33} versus cell ratio c/a for these systems are also indicated in Fig. 3 as red squares. They follow the overall trend of the $Zn_{15}YO_{15}N$ alloy (displayed in Fig. 3 as filled red circles). This behavior supports the assumption that an enhanced PE performance is to be expected in a wurtzite structure when c/a is reduced and approaching a phase transition as Momida and Oguchi suggested [13]. Moreover, it reveals that the linear relation no longer holds, a result that can be compared to the calculations in Ref. [14].

IV. DISCUSSION

The overall set of results presented in Sec. III indicates that to fully optimize the PE response of ZnO-based alloys, one has to consider the nature of the substituents, their concentration, and the in-plane strain value. We also highlighted that the PE properties increase when approaching the wurtzite to hexagonal phase transitions by varying these parameters.

A. Potential PE performance estimation by structural calculations

The results in Fig. 3 clearly demonstrate a linear relationship between e_{33} and c/a values, independent of the nature of the substituents, their concentration, and the strain value as long as the system is not too close to the wurtzite to hexagonal phase transition. This result is in line with the observations of Momida and Oguchi [13] for other wurtzite systems.

This observation allows for the rapid screening of potentially interesting ZnO-based alloys, thereby reducing the need for time consuming DFPT calculations. It also enables one to "predict" the properties of alloys that do not exhibit a DFT band gap. Indeed, straightforward DFT calculations are sufficient to determine c/a values which can then be reported on the graph in Fig. 3 to establish a first estimate for e_{33}. The most promising system could then be further investigated using full DFPT calculations and, eventually, experiments.

We have computed the $2 \times 2 \times 2$ supercell cell ratio c/a for transition metals substitutions, as described in our methodology. The obtained cell ratios were then used to estimate the PE performance of the alloys. The procedure is illustrated

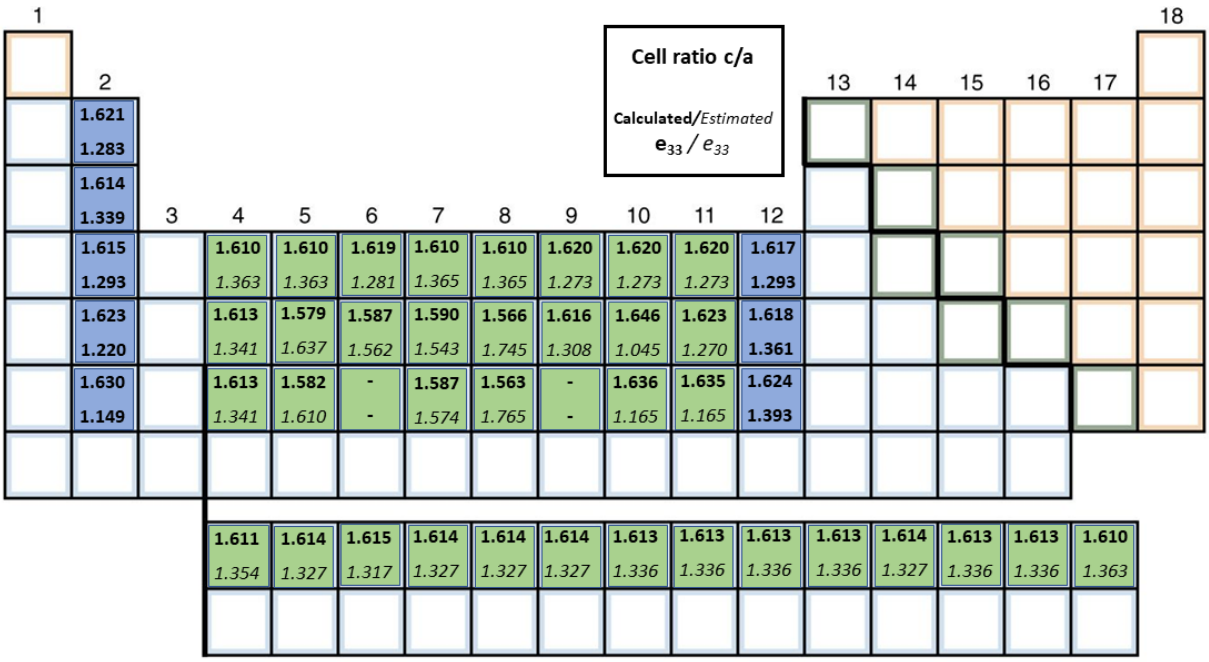

FIG. 5. Periodic table indicating the calculated cell ratios c/a (upper value) and e_{33} coefficient in C m^{-2} (lower value) for ternary $Zn_{15}XO_{16}$ alloys at the position of element X. The estimated e_{33} coefficient values for alloys which do not exhibit a sufficiently large DFT bandgap have been interpolated as shown in Fig. 3 and are indicated in italics in the table. For visibility purposes, the alloys for which e_{33} has been estimated display a green background and those corresponding to calculated e_{33} display a blue background.

in Fig. 3 for the eighth column of the periodic table (Fe, Ru, and Os), as indicated by the dotted lines. The very low cell ratio calculated for $Zn_{15}RuO_{16}$ and $Zn_{15}OsO_{16}$ points to an e_{33} coefficient in the range of $e_{33} \approx 1.75$ C m^{-2}, a large (37%) improvement over the equivalent coefficient calculated for pristine ZnO. The cell ratio remains above $c/a = 1.5$, indicating that the data is in the linear regime described by Momida and Oguchi [13].

Figure 5 presents a synthesis, in a form reproducing the periodic table of elements, of the computed c/a and predicted e_{33} values for ternary alloys incorporating corresponding elements. In each cell of this periodic table, the upper number is the computed c/a value while the predicted e_{33} (in C m^{-2}) is depicted at the bottom. All data correspond to the substitution of one atom in 32-atom supercells. For example, the substitution of one Zn atom with Ti yields a c/a value of 1.61 which corresponds, after interpolation using Fig. 3, to a predicted e_{33} of 1.363 C m^{-2}.

The general trend among the transition metals shows a small improvement in the e_{33} coefficient for the 10 elements at the top full row of the periodic table. However, the second and third rows underneath display more variations, with some alloys exhibiting little to no performance improvement as in the case of $Zn_{15}ZrO_{16}$ and $Zn_{15}HfO_{16}$. At the opposite range of the spectrum, $Zn_{15}RuO_{16}$ (eighth column, second row) and $Zn_{15}OsO_{16}$ (directly underneath) display the smallest cell ratio in all calculated unstrained alloys ($c/a = 1.563$) corresponding to $e_{33} \approx 1.765$ C m^{-2}.

According to our computations on strained $Zn_{15}YO_{15}N$, these values remain in the linear domain, which gives us confidence that they are experimentally attainable. The relatively poor performance of $Zn_{15}VO_{16}$ is consistent with the conclusions of Nakamura *et al.* conclusions concerning relaxed compounds [14]. The same can be said of the significant improvement concerning the cell ratio of $Zn_{15}NbO_{16}$ and $Zn_{15}TaO_{16}$ (fifth column, second and third row, respectively) pointing to high PE coefficients e_{33}, as reported once again by Nakamura *et al.* [14].

We also compiled in Fig. 5 the results of our simulations for alloys incorporating lanthanides. The lanthanides substitutions did not reveal any noticeable difference concerning the cell ratio c/a most likely because the variability between the lanthanides is mainly on the $4f$ shell of electrons as well as the lanthanides contraction. However, the possibility remains that the description of the f electron in the JTH Library might be a source of error, as these $4f$ electrons are delocalized and treated as plane waves. We chose to use them nonetheless for the sake of allowing comparison between datasets of the same library on the assumption that the f electrons should not have a major impact on the structural parameters. Further studies would benefit from investigating this localization effect of the f electrons.

In Sec. III B we remarked that for $Zn_{15}YO_{15}N$ alloys a linear (positive) correlation has been established between the stiffness coefficient C_{33} and the cell ratio c/a (see Fig. 2 in the Supplemental Material [31]). This observation, should it be verified for other conditions (concentration, substituent, higher strain), would allow for the same strategy as the one proposed above to estimate the C_{33} coefficient of alloys without the need of a DFPT calculation.

If such an estimation is indeed possible, it would also allow us to estimate the effective $d_{33\,\mathrm{eff}}$ coefficient, a lower bound of

d_{33} useful for thin film applications and defined by [34]

$$d_{33\,\mathrm{eff}} = \frac{e_{33}}{C_{33}^{E}}, \tag{4}$$

complementing our proposed approach to provide a quick insight on the PE performances of candidate alloys. It would be particularly interesting for further studies to investigate more in depth these linear relations, for instance by investigating at higher substituents concentrations or with bigger systems.

B. Impact of concentration and strain on tensor symmetries

A careful analysis of the stiffness and PE tensors for the higher concentration Zn_7YO_7N alloys reveal that the expected symmetries are not respected, in sharp contrast with our results for the other materials systems and substituent concentration. More specifically, some coefficients had finite values while null values were expected.

This result indicates that the combination of substitution and strain drives the alloy too far from pristine ZnO for it to entirely retain its crystalline wurtzite symmetry. As we explained before, the Zn_7YO_7N alloy naturally relax in a hexagonal structure; it only displays PE properties when maintained in a wurtzite structure by an applied biaxial in plane strain. Therefore, investigating higher concentrations of Y and N substituents should not yield interesting results as the growing concentration of substituents would take us further away from the phase transition and the wurtzite structure. In the specific case of Zn_7YO_7N alloy, the interest of further increasing the concentration is probably meager. However, it should not necessarily be the case for other substituents.

C. Nonlinearity close to the wurtzite/hexagonal phase transition

We demonstrated in Fig. 3 that the Zn_7YO_7N alloy (which relaxes in the hexagonal structure for the unstrained system) can be maintained in a wurtzite structure by applying a compressive biaxial strain. Moreover, this proximity with a phase transition gave rise to the largest PE coefficients e_{33} reported in this study.

Indeed, Fig. 3 indicates that the relationship between e_{33} and c/a becomes superlinear at low c/a values, close to the wurtzite-to-hexagonal phase transition. The nonlinear part of the e_{33} versus c/a graph could perhaps be described with an approach similar to critical exponents [35]. This theory predicts the behavior of systems close to a phase transition, more specifically the evolution of physical properties (here the e_{33} coefficient) versus a control parameter (here analogous to the cell ratio c/a). In the context of this theory, the physical properties follow a power law of the control parameter in the vicinity of the phase transition. This would explain the behavior observed by Nakamura *et al.* [14], who attributed the sharp decline in PE performance at strain values in the vicinity of 6–7% to a transition from a wurtzite structure to a hexagonal structure. The steep increase of e_{33} versus the applied strain near 6–7% could be explained by a critical exponent approach. The abrupt drop to zero in e_{33} observed in Ref. [14] above a threshold strain value coincides with a materials system occurs because we reach a structure with an inversion symmetry due to the phase transition. Because of this symmetry, the obtained system cannot display any net PE properties. This is coherent with Momida and Oguchi's Fig. 2 that highlights a phase transition between wurtzite and hexagonal phases below a certain cell ratio (systematically smaller than the ones studied here). The effect of large strain values on the PE coefficient e_{33} seems to depend, according to Nakamura *et al.* [14], on the nature of the substituent (see again Fig. 9 of Ref. [14]), with the best results obtained for $Zn_{15}VO_{16}$. This substituent dependence can be explained by the proximity of the phase transition, where minor parametric changes can significantly impact the properties of the material.

V. CONCLUSION

We have calculated the piezoelectric and stiffness tensors of 32-atom supercells for a large number of ZnO-based alloys using *ab initio* DFPT simulations with the LDA functional. Low concentration for substituents to either Zn, O or both were considered on unstrained and biaxially strained systems. The d_{33} coefficient for unstrained $Zn_{15}YO_{15}N$ and $Zn_{15}LaO_{15}N$ alloys are, respectively, 17.5 and 18 pC N^{-1}, whereas e_{33} is 1.7 C m^{-2} for both alloys. These values are significantly improved compared to simulated values for pristine ZnO ($d_{33} = 11.4$ pC N^{-1} and $e_{33} = 1.3$ C m^{-2}). Applying 2% tensile strain on $Zn_{15}YO_{15}N$ results in an increase of the e_{33} coefficient to 2.1 C m^{-2}, a 60% increase over pristine ZnO.

We confirm for a variety of ternary and quaternary ZnO-based alloys that a linear relationship between the e_{33} coefficient and the cell ratio c/a is verified, with a slope of ≈ -9 C m^{-2}. Our results also indicate that the PE coefficients follow the same trends with respect to changes in c/a caused by variations in chemical composition or by applying biaxial strain. Based on this correlation, we proposed a simple method to identify promising candidates among PE alloys in the wurtzite family, effectively reducing the intensive computational resources needed to obtain optimal PE performance for applications compatible with the many requirements of thin film growth and processing.

ACKNOWLEDGMENTS

This research was financially supported by the Natural Sciences and Engineering Research Council of Canada (NSERC), under the Discovery Grants program. grant No. RGPIN-2016-06666 (M.C.) and RGPIN-2016-06417 (R.A.M.). Computations were made on the supercomputers MP2 and MP2b from Université de Sherbrooke, managed by Calcul Québec (www.calculquebec.ca) and Compute Canada (www.computecanada.ca, http://dx.doi.org/10.13039/100013020). The operation of this facility is funded by the Canada Foundation for Innovation (CFI), the ministère de l'Économie et de l'Innovation du Québec (MESI, http://dx.doi.org/10.13039/100013688), and the Fonds de recherche du Québec Nature et technologies (FRQ-NT, http://dx.doi.org/10.13039/501100003151).

[1] J. A. B. Gripp and D. A. Rade, Mech. Syst. Signal Process. **112**, 359 (2018).

[2] E. Benes, M. Gröschl, W. Burger, and M. Schmid, Sens. Actuat. A Phys. **48**, 1 (1995).

[3] C. Fei, X. Liu, B. Zhu, D. Li, X. Yang, Y. Yang, and Q. Zhou, Nano Energy **51**, 146 (2018).

[4] N. Izyumskaya, Y. I. Alivov, S. J. Cho, H. Morkoç, H. Lee, and Y. S. Kang, Crit. Rev. Solid State Mater. Sci. **32**, 111 (2007).

[5] M. T. Todaro, F. Guido, V. Mastronardi, D. Desmaele, G. Epifani, L. Algieri, and M. De Vittorio, Microelectron. Eng. **183–184**, 23 (2017).

[6] B. Sahoo, V. A. Jaleel, and P. K. Panda, Mater. Sci. Eng. B Solid-State Mater. Adv. Technol. **126**, 80 (2006).

[7] T. R. Shrout and S. J. Zhang, J. Electroceram. **19**, 185 (2007).

[8] Y. C. Yang, C. Song, F. Zeng, F. Pan, Y. N. Xie, and T. Liu, Appl. Phys. Lett. **90**, 1 (2007).

[9] Y. C. Yang, C. Song, X. H. Wang, F. Zeng, and F. Pan, Appl. Phys. Lett. **92**, 012907 (2008).

[10] Y. C. Yang, X. J. Liu, F. Zeng, F. Pan, and C. Song, Mater. Sci. Eng. R Reports **62**, 1 (2008).

[11] S. Goel, N. Sinha, H. Yadav, S. Godara, A. J. Joseph, and B. Kumar, Mater. Chem. Phys. **202**, 56 (2017).

[12] S. Goel, N. Sinha, H. Yadav, A. J. Joseph, and B. Kumar, Phys. E Low-Dimensional Syst. Nanostruct. **91**, 72 (2017).

[13] H. Momida and T. Oguchi, Appl. Phys. Express **11**, 041201 (2018).

[14] K. Nakamura, S. Higuchi, and T. Ohnuma, J. Appl. Phys. **119**, 114102 (2016).

[15] D. R. Hamann, X. Wu, K. M. Rabe, and D. Vanderbilt, Phys. Rev. B **71**, 035117 (2005).

[16] X. Gonze, F. Jollet, F. Abreu Araujo, D. Adams, B. Amadon, T. Applencourt, C. Audouze, J.-M. Beuken, J. Bieder, A. Bokhanchuk, E. Bousquet, F. Bruneval, D. Caliste, M. Côté, F. Dahm, F. Da Pieve, M. Delaveau, M. Di Gennaro, B. Dorado, C. Espejo, G. Geneste, L. Genovese, A. Gerossier, M. Giantomassi, Y. Gillet, D. R. Hamann, L. He, G. Jomard, J. Laflamme Janssen, S. Le Roux, A. Levitt, A. Lherbier, F. Liu, I. Lukačević, A. Martin, C. Martins, M. J. T. Oliveira, S. Poncé, Y. Pouillon, T. Rangel, G.-M. Rignanese, A. H. Romero, B. Rousseau, O. Rubel, A. A. Shukri, M. Stankovski, M. Torrent, M. J. Van Setten, B. Van Troeye, M. J. Verstraete, D. Waroquiers, J. Wiktor, B. Xu, A. Zhou, and J. W. Zwanziger, Comput. Phys. Commun. **205**, 106 (2016).

[17] F. Jollet, M. Torrent, and N. Holzwarth, Comput. Phys. Commun. **185**, 1246 (2014).

[18] P. E. Blöchl, Phys. Rev. B **50**, 17953 (1994).

[19] M. Torrent, F. Jollet, F. Bottin, G. Zérah, and X. Gonze, Comput. Mater. Sci. **42**, 337 (2008).

[20] H. J. Monkhorst and J. D. Pack, Phys. Rev. B **13**, 5188 (1976).

[21] C. G. Broyden, IMA J. Appl. Math. **6**, 222 (1970).

[22] R. D. King-Smith and D. Vanderbilt, Phys. Rev. B **47**, 1651 (1993).

[23] F. Bruneval, J. P. Crocombette, X. Gonze, B. Dorado, M. Torrent, and F. Jollet, Phys. Rev. B: Condens. Matter Mater. Phys. **89**, 045116 (2014).

[24] A. Py-Renaudie, Propriétés Piézoélectriques Des Alliages d'oxyde de Zinc: Étude *Ab-Initio*, Polytechnique Montréal, 2019, https://publications.polymtl.ca/3973/.

[25] E. S. Goh, J. W. Mah, and T. L. Yoon, Comput. Mater. Sci. **138**, 111 (2017).

[26] J. P. Perdew, Int. J. Quantum Chem. **28**, 497 (2009).

[27] R. Resta and D. Vanderbilt, in *Physics of Ferroelectrics* (Springer, Berlin/Heidelberg, 2007), pp. 31–68.

[28] X. Wu, D. Vanderbilt, and D. R. Hamann, Phys. Rev. B **72**, 035105 (2005).

[29] N. Troullier and J. L. Martins, Phys. Rev. B **43**, 1993 (1991).

[30] M. Cococcioni and S. de Gironcoli, Phys. Rev. B **71**, 035105 (2005).

[31] See Supplemental Material at http://link.aps.org/supplemental/10.1103/PhysRevMaterials.4.053601 for raw data on piezoelectric and stiffness tensors, as well as a discussion on the correlation between the C_{33} coefficient and the cell ratio c/a.

[32] J. Y. Tsao, *Materials Fundamentals of Molecular Beam Epitaxy* (Elsevier, Amsterdam, 1993).

[33] A. Dal Corso, M. Posternak, R. Resta, and A. Baldereschi, Phys. Rev. B **50**, 10715 (1994).

[34] V. Lindroos, A. Lehto, T. Motooka, and M. Tilli, *Handbook of Silicon Based MEMS Materials and Technologies* (Elsevier, Amsterdam, 2010).

[35] M. E. Fisher, Phys. Rev. **176**, 257 (1968).

[36] T. M. Sabine and S. Hogg, Acta Crystallogr. Sect. B Struct. Crystallogr. Cryst. Chem. **25**, 2254 (1969).

[37] D. F. Nelson, editor, *Piezoelectric, Pyroelectric, and Related Constants* (Springer-Verlag, Berlin/Heidelberg, 1993).